Author Manuscript

Development of a Slow-Degrading Polymerized Curcumin Coating for Intracortical Microelectrodes

Alexis M. Ziemba,

Department of Biomedical Engineering and Center for Biotechnology and Interdisciplinary Sciences, Rensselaer Polytechnic Institute, Troy 12180-3590 New York, United States; Neuroscience Program, Department of Biological Sciences, Smith College, Northampton 00000 Massachusetts, United States

Mary Clare Crochiere Woodson,

Department of Biomedical Engineering and Center for Biotechnology and Interdisciplinary Sciences, Rensselaer Polytechnic Institute, Troy 12180-3590 New York, United States; Present Address: The Carle Illinois College of Medicine, Urbana, Illinois, United States

Jessica L. Funnell,

Department of Biomedical Engineering and Center for Biotechnology and Interdisciplinary Sciences, Rensselaer Polytechnic Institute, Troy 12180-3590 New York, United States

Douglas Wich,

Department of Biomedical Engineering and Center for Biotechnology and Interdisciplinary Sciences, Rensselaer Polytechnic Institute, Troy 12180-3590 New York, United States; Present Address: Tufts University, Medford, Massachusetts, United States

Bailey Balouch,

Center for Biotechnology and Interdisciplinary Sciences, Rensselaer Polytechnic Institute, Troy 12180-3590 New York, United States; Present Address: Drexel University College of Medicine, Philadelphia, Pennsylvania, United States

Corresponding Authors: **Edmund F. Palermo** – *Department of Materials Science and Engineering, Rensselaer Polytechnic Institute, Troy 12180-3590 New York, United States;* palere@rpi.edu; **Ryan J. Gilbert** – *Department of Biomedical Engineering and Center for Biotechnology and Interdisciplinary Sciences, Rensselaer Polytechnic Institute, Troy 12180-3590 New York, United States;* gilber2@rpi.edu.

Author Manuscript

Deniz Rende,

Center for Materials, Devices, and Integrated Systems, Rensselaer Polytechnic Institute, Troy 12180-3590 New York, United States

Dahlia N. Amato,

Department of Materials Science and Engineering and Center for Biotechnology and Interdisciplinary Sciences, Rensselaer Polytechnic Institute, Troy 12180-3590 New York, United States; Present Address: CertainTeed, Malvern, Pennsylvania, United States

Jonathan Bao,

Center for Biotechnology and Interdisciplinary Sciences, Rensselaer Polytechnic Institute, Troy 12180-3590 New York, United States; Present Address: Albany Medical College, Albany, New YorY, United States

Ingrid Oprea,

Center for Biotechnology and Interdisciplinary Sciences, Rensselaer Polytechnic Institute, Troy 12180-3590 New York, United States; Present Address: Regeneron Pharmaceuticals, Rensselaer, New YorY, United States

Dominica Cao,

Neuroscience Program, Department of Biological Sciences, Smith College, Northampton 00000 Massachusetts, United States; Present Address: Yale University, New Haven, Connecticut, United States

Neda Bajalo,

Center for Biotechnology and Interdisciplinary Sciences, Rensselaer Polytechnic Institute, Troy 12180-3590 New York, United States; Present Address: Experimur, Chicago, Illinois, United States

Evon S. Ereifej,

Veteran Affairs Ann Arbor Healthcare System, Ann Arbor 00000 Michigan, United States; Department of Biomedical Engineering and Department of Neurology, University of Michigan, Ann Arbor 00000 Michigan, United States; United States Advanced Platform Technology Center, Louis Stokes Cleveland Veterans Affairs Medical Center, Cleveland 44106 Ohio, United States

Jeffrey R. Capadona,

United States Advanced Platform Technology Center, Louis Stokes Cleveland Veterans Affairs Medical Center, Cleveland 44106 Ohio, United States; Department of Biomedical Engineering, Case Western Reserve University, Cleveland 44106 Ohio, United States

Edmund F. Palermo,

Department of Materials Science and Engineering, Rensselaer Polytechnic Institute, Troy 12180-3590 New York, United States

Ryan J. Gilbert

Department of Biomedical Engineering and Center for Biotechnology and Interdisciplinary Sciences, Rensselaer Polytechnic Institute, Troy 12180-3590 New York, United States

Abstract

Intracortical microelectrodes are used with brain–computer interfaces to restore lost limb function following nervous system injury. While promising, recording ability of intracortical microelectrodes diminishes over time due, in part, to neuroinflammation. As curcumin has demonstrated neuroprotection through anti-inflammatory activity, we fabricated a 300 nm-thick intracortical microelectrode coating consisting of a polyurethane copolymer of curcumin and polyethylene glycol (PEG), denoted as poly(curcumin-PEG$_{1000}$ carbamate) (PCPC). The uniform PCPC coating reduced silicon wafer hardness by two orders of magnitude and readily absorbed water within minutes, demonstrating that the coating is soft and hydrophilic in nature. Using an in vitro release model, curcumin eluted from the PCPC coating into the supernatant over 1 week; the majority of the coating was intact after an 8-week incubation in buffer, demonstrating potential for longer term curcumin release and softness. Assessing the efficacy of PCPC within a rat intracortical microelectrode model in vivo, there were no significant differences in tissue inflammation, scarring, neuron viability, and myelin damage between the uncoated and PCPC-coated probes. As the first study to implant nonfunctional probes with a polymerized curcumin coating, we have demonstrated the biocompatibility of a PCPC coating and presented a starting point in the design of poly(pro-curcumin) polymers as coating materials for intracortical electrodes.

Graphical Abstract
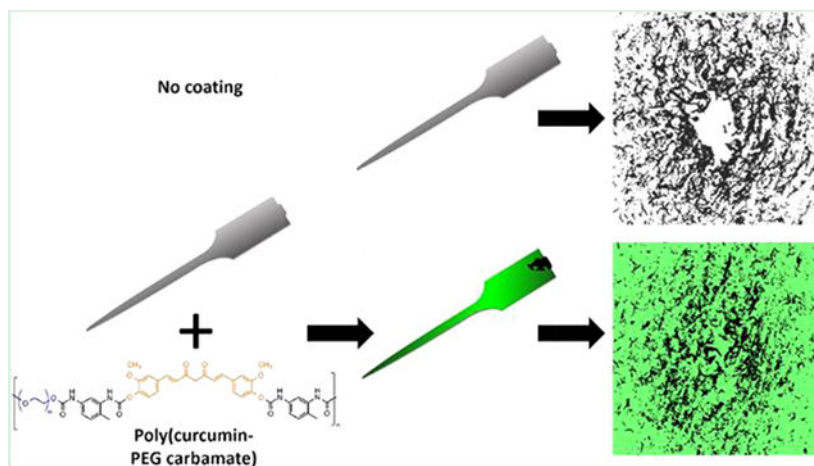
Keywords

electrode; curcumin; polyethylene glycol; coating; drug delivery; polyprodrug

1. INTRODUCTION

Intracortical electrode implants have been implemented in the clinic to restore auditory function, provide artificial vision systems, manage epileptiform activity, and increase mobility in cases of amputation and paralysis.[1] Even with remarkable recent advances, recording instability due to the neuroinflammatory response following electrode implantation remains a major challenge.[1–4] Acutely after injury, microglia and blood-born macrophages are recruited to phagocytose cellular debris. These recruited macrophages

secrete damaging pro-inflammatory factors and reactive oxygen species that lead to local neuron and glia cell death.[2,5–9] In an attempt to stabilize the interface between the implanted electrode and host tissue, reactive astrocytes form a glial scar around the electrode 2 weeks postimplantation,[2,5,7,10–12] potentially impeding ion diffusion which would hinder electrode recording ability long term. Ultimately, the injury response to intracortical electrode implantation leads to neurodegeneration,[5,6,12–14] leading to impaired recording ability.

As neuroinflammation contributes to electrode recording instability, many approaches use systemic delivery of pharmacological agents to reduce neuroinflammation.[15–18] However, major limitations of systemic drug delivery are (1) unwanted side effects through interactions peripheral to the injury site, such as abdominal lesions from repeated intra-peritoneal resveratrol administration,[19] and (2) low drug concentrations at the target brain tissue due to the restrictive blood–brain barrier.[20] To provide local delivery and minimize systemic side effects, studies have applied therapeutic coatings to intracortical microelectrodes, such as dexamethasone encapsulated into nitrocellulose layers,[21] interleukin-1 receptor agonist (IL-1Ra)-incorporated poly(ethylene glycol) (PEG)-maleimide coatings,[22] and cyclodextrin polymers loaded with resveratrol.[23] While these approaches deliver drugs locally to the implant site, some coatings where drugs are incorporated through mixing with a polymer, release drug quickly through a burst release, are limited by the amount of cargo the carrier polymer matrix can hold, and are unable to provide long-term drug delivery to help mitigate chronic inflammation.

Curcumin (1,7-bis(4-hydroxy-3-methoxyphenyl)-1,6-heptadiene-3,5-dione) is a polyphenolic antioxidant found in the spice turmeric from the ginger plant family, *Curcuma longa*.[24] Curcumin broadly mitigates inflammation and oxidative stress and has been studied globally as a treatment for arthritis, cancer, bacterial infection, and metabolic syndrome.[24,25] Curcumin mediates oxidative stress via its hydrogen atoms α to both ketones[26] and the phenol moieties[27] (Figure 1A). Various in vitro and in vivo nervous system injury models have demonstrated curcumin's ability to protect cells against peroxynitrite damage,[28] lipid peroxidation,[29] and malondialdehyde and nitric oxide levels.[30] Additionally, curcumin targets microglia and canonical inflammatory pathways in vitro; curcumin increased expression of anti-inflammatory markers IL-4, IL-10, and arginase-1,[31] decreased proinflammatory markers including inducible nitric oxide synthase, IL-1, and tumor necrosis factor-α,[31–34] and suppressed the JAK/STAT pathway[31,35] in the BV-2 microglial cell line. These antioxidant and anti-inflammatory properties may provide neuroprotection following nervous system injury from electrode implantation.

To our knowledge, two studies applied curcumin directly to intracortical implant models, including polymer implants consisting of poly(vinyl alcohol), cellulose nanocrystals, and curcumin (either 1 or 3% w/w)[36] and poly(vinyl acetate), cellulose nanocrystals, and curcumin (0.01% w/w) implants.[37] In both cases, the curcumin-containing materials were created to reduce inflammation following implantation due to curcumin's antioxidant characteristics and from the mechanically adaptive capability of the cellulose nanocrystals. The 0.01% (w/w) curcumin/PVAc composite material was less effective in preserving neuron density 2 weeks postimplantation, compared to 0.01% (w/w) resveratrol containing counterparts. However, Potter et al. observed greater neuron density proximal to the

PVAc implant as well as a more stable blood–brain barrier compared to implants without curcumin, though this improvement was not observed 12 weeks postimplantation.[36] As implants of Potter et al. released almost all of the curcumin over the first 10 h,[36] extended delivery of curcumin to target chronic injury phenomena would need to be achieved through alternative strategies.

Direct polymerization of curcumin within the polymer backbone may minimize a burst release, and the release rate may be modified by altering the chemistry used in the polymerization. Furthermore, polymerization of curcumin may increase drug loading efficiency, (2) stabilize curcumin, and (3) alter water solubility based on the polymer composition. As curcumin is a diol, a number of studies have synthesized polymers containing curcumin in the backbone.[38–41] As polymerized drugs are a promising approach for therapeutic intracortical electrode coatings, we aimed to create a curcumin polymer that was biodegradable and hydrophilic while preserving curcumin bioactivity and ensuring a sustained local delivery of curcumin; thus, we developed a polymerized curcumin therapeutic via carbamate linkages, as these linkages were used in the development of other prodrug polymers.[42]

In the current study, poly(pro-curcumin-PEG$_{1000}$ carbamate) (PCPC) was synthesized via step-growth polymerization with toluene diisocyanate (Figure 1A). PEG was incorporated to increase polymer hydrophilicity and promote fusogen activity to repair damaged membranes,[43] while the carbamate linkages were incorporated to enable biodegradability on a timescale of months to years.[44] After nonfunctional Michigan-style single shank probes and silicon wafers were dip coated in a PCPC solution, coatings were assessed for uniformity and thickness, mechanical properties, water absorption and swelling, and degradation. After demonstrating material characteristics appropriate for in vivo testing, the PCPC-coated probes were implanted into the rat cortex for 2 weeks, and neuroinflammation, glial scarring, neuron loss, myelination, and implant site area were assessed using immunohistochemistry. We hypothesized that the PCPC coating would exhibit anti-inflammatory activity, thereby reducing inflammation, glial scarring, and neuron loss proximal to the probe. To our knowledge, this study is the first to implant nonfunctional probes with a poly(pro-curcumin) coating into a preclinical animal model and see similar biocompatibility to the silicon probe.

2. EXPERIMENTAL SECTION

All materials and cell culture product information (Table S1), surgical and histological product information (Table S2), drug product and dosing information (Table S3), and equipment and software information (Table S4) are presented in the Supporting Information. This work was conducted as described previously.[45]

2.1. PCPC Synthesis and Characterization.

PEG$_{1000}$ was placed into a 140 °C vacuum oven for 48 h to remove moisture, prior to transfer into a nitrogen-purged glove box. Within a 25 mL round bottom flask, PEG (2.844 g) was heated at 60 °C for 30 min prior to the addition of curcumin (1.084 g) and dibutyltin dilaurate (0.098 g). Anhydrous tetrahydrofuran (THF; 5 mL) was added to the mixture and

allowed to stir for 20 min. In a scintillation vial, toluene diisocyanate (TDI, 1.00 g) was mixed with THF (2 mL). The TDI solution was transferred to the round bottom flask, and the scintillation vial was rinsed and then transferred to a round bottom flask two times with 2 mL of THF to ensure that all the isocyanate is added fully to the reaction mixture. The reaction mixture was then stirred at 50 °C for 12 h. The product became a viscous orange solution which was then precipitated into MeOH. The gummy precipitate was then placed into a scintillation vial and under vacuum to remove residual solvents for 48 h to yield 3.32 g.

The dried polymer was dissolved in DMSO-d_6 for proton nuclear magnetic resonance (^{1}H NMR) (Bruker 800 MHz NMR) to confirm polymer identity. For gel permeation chromatography (GPC), PCPC was dissolved in THF and molecular weight was determined using a Tosoh EcoSEC Elite GPC System (100 μL injection volume, 1 mL min^{-1} flow rate). For differential scanning calorimetry (DSC), a TA Instruments DSC-Q100 was used to assess the thermal properties of PCPC. Briefly, PCPC (6.45 mg) was hermetically sealed in an aluminum pan. The sample was equilibrated to −60 °C and then heated to 150 °C at a rate of 10 °C min^{-1}. The glass transition temperature (T_g) was determined by analyzing the heating curves using TA Universal Analysis Software.

2.2. Dip Coating Nonfunctional Probes and Wafer with PCPC.

Nonfunctional single shank Michigan-style silicon (Si) probe (dimensions 2 mm × 123 μm × 15 μm) fabrication (based on previously described methods[46]) and polymer synthesis methods are described in the Supporting Information. A 5% (w/w) solution of PCPC was prepared in chloroform and stirred overnight. Each probe was plasma cleaned for 1.5 min, and the tab was secured to Dumont SS fine forceps attached to a Stoelting stereotaxic device (Figure S1). The probe was lowered into PCPC solution and removed at a rate of approximately 0.4 mm s^{-1}. Probes were dried in air with the shaft suspended on a piece of tape. For material coating characterizations in which probes could not be used (due to the small size of the shank), 5 × 10 mm Si wafers were dip-coated by hand for material characterization tests using the same approximate withdrawal rate. Coated probes and wafers were stored under vacuum and protected from light to prevent hydrolytic degradation and compromised bioactivity, respectively. Probes used for animal experiments were sterilized via ethylene oxide.

2.3. PCPC Probe Coating Uniformity and Swelling Characterization by Microscopy.

PCPC coating uniformity and swelling characterization was performed using an FEI Versa 3D Dual Beam scanning electron microscope (SEM). Probes were first sputter-coated with an approximately 0.5 nm layer of Au/Pd using a Hummer V Technics sputter coater. The coating was visualized using a 2 kV electron beam, 5.0 spot size, and a working distance of 10 mm. Images were taken at 66× to image the top surface of the entire probe. Images of the side of the probe were taken at 6500× to assess the uniformity on the side surface as well. One probe from each coating batch was imaged and analyzed (n = 4 probe). Each batch is defined as using a newly prepared polymer solution for dip coating less than 1 week prior to implantation. To ensure that there was minimal swelling of the PCPC coating (as swelling could cause tissue damage), n = 3 probes were imaged 1 week following incubation

in diH$_2$O at 37 °C; diH$_2$O was used instead of physiologically relevant buffers to prevent salt crystallization on the probe.

Coating uniformity and swelling were also assessed using an Olympus IX-81 Confocal Microscope and Metamorph Premier 7.7.3.0 imaging software. Using curcumin's native fluorescence, images were taken at an emission wavelength of $\lambda_{EM} = 550$ nm, at an exposure of 100 ms, and using a gain of 100. To assess uniformity, fluorescence and brightfield images were taken at 4× to obtain the top view of the probe. A minimum of one probe from each batch was imaged and analyzed ($n = 6$ probes) to ensure coating consistency between batches. To further assess swelling after submersion in PBS, the side surface of probes was imaged at 40× magnification. Images were captured immediately after submersion following 15 min of incubation in PBS, when water absorption equilibrium was reached ($n = 2$ probes).

2.4. Quantification of PCPC Surface Area Coverage on the Probe.

To quantify the total area covered by the probe coating, FIJI software was used to outline the boundaries of each probe using a binary mask from the brightfield channel image. The region representing the probe was quantified using the analyze particle function (minimum size threshold = 50,000). To quantify the total area covered by the PCPC coating, the fluorescent regions indicating coating were outlined and quantified using the analyze particle function (minimum size threshold = 5). Results are reported as the mean percent area covered ± standard error of the mean ($n = 6$ probes from three batches).

2.5. PCPC Coating Nanoindentation on Silicon Wafer.

Nanoindentation experiments were performed using a Hysitron TriboIndenter with a load resolution of 100 nN, a displacement resolution of 1 nm, and a maximum indentation depth of 5 μm. A Berkovich tip with a 100 nm radius was used. Quasi-static displacement-controlled nanoindentation testing was performed with a displacement vs time profile, a 4-nm s^{-1} loading and unloading rate, and a 20 nm peak (10-s total time profile) at room temperature (RT). Before and after each test, the standard quartz sample was also tested with the same load function parameters. Each specimen was tested with 12 indents (4 × 3 grid with 10-μm separation) on $n = 3$ Si and $n = 3$ PCPC-coated Si wafers. The reduced modulus (E_r) and hardness (H) of the indents were calculated using the Hysitron TriboIndenter's data analysis software. The values for the technical replicate indents on each sample were averaged, and then the sample means were averaged. Results were plotted as the mean E_r or H (GPa) ± standard error of the mean.

2.6. PCPC Water Absorbance on Silicon Wafer.

Using a Kruss DSA100 Drop Shape Analyzer, the wetting/water absorption equilibrium of the PCPC coating was assessed. A 3 μL droplet of water was applied to Si and PCPC-coated Si wafers. An image was captured immediately and every 30 s thereafter for up to 15 min. The static water contact angle was then measured using the Kruss DSA100 software until the PCPC coating began to absorb water and assume an irregular shape. The mean contact angle (average of the right and left sides of the water droplet) was calculated at each timepoint and averaged with the other wafer replicates ($n = 3$–5 different wafers were

used for each surface condition). The mean contact angle (± standard error of the mean) was plotted as a function of time.

2.7. PCPC Silicon Wafer Coating Degradation/Dissolution into the Supernatant.

PCPC dip-coated Si wafers (5×10 mm) were incubated in PBS (1 mL) in a 37 °C, 95% air/5% CO_2 incubator. The supernatant was collected at 4 and 8 h, 1, 2, 5, 8, and 11 days, and 2, 3, 4, 5, 6, and 8 weeks postincubation. The supernatant was replaced with PBS (1 mL) at each time point. The supernatants were stored at −20 °C until they were lyophilized, resuspended in 100% ethanol, and centrifuged down at 10,000 rpm for 30 s at 4 °C to pellet the salts. A standard curve using PCPC in 100% ethanol was made and measured using a Tecan M200 plate reader. The fluorescence intensity of each sample was plotted as mean total soluble PCPC release products in nmol (± standard error of the mean) against time ($n = 3–4$ wafers per time point).

2.8. PCPC Silicon Wafer Coating Degradation/Dissolution by Confocal Microscopy.

To quantify the amount of PCPC remaining on the Si wafer after incubation, PCPC-coated wafers at parallel time points to supernatant measurements (0, 1, 2, and 8 weeks) were imaged using an Olympus IX-81 Confocal Microscope and Metamorph Premier 7.7.3.0 imaging software. Using curcumin's native fluorescence, 10× images of five different fields of view (FoV) on each wafer ($n = 3$ wafers per time point) were captured (at an emission wavelength, $\lambda_{EM} = 550$ nm) with an exposure of 100 ms and a gain of 100. For each field of view, the mean fluorescence intensity (MFI) was determined using the histogram tool in ImageJ for 500×500 μm regions. The average MFI for each wafer was calculated. As dark voids in the coatings of incubated wafers were observed, the supernatant was also imaged using confocal microscopy at 40× magnification for each time point.

2.9. Antioxidant Activity of PCPC by 2,2-Diphenyl-1-picrylhydrazyl (DPPH).

Antioxidant activity of the polymer was confirmed using a DPPH assay. DPPH is a radical compound that readily reacts with antioxidant compounds and subsequently loses its purple hue. A 100 μg mL^{-1} solution of DPPH was prepared in 100% ethanol. An absorbance spectrum was collected using a Tecan M200 plate reader, $\lambda = 200–800$ nm. A 16-ng piece of PCPC was placed into the DPPH solution and put on a shake plate at a setting of 250 rpm. After 30 min, a dramatic color change from purple to yellow was observed, and the absorbance spectrum was collected again. The absorbance spectrum of PCPC alone was used as a control.

2.10. Nonfunctional Probe Implantation Procedure.

Approval for surgical procedures was granted by the Institutional Animal Care and Use Committee (IACUC) at Rensselaer Polytechnic Institute. Male ($n = 7$) and female ($n = 6$) 9-week old Sprague Dawley rats were used for the procedures.[47] Animals were given a carprofen cup to provide analgesia the day prior surgical procedures. Anesthesia was induced with an EZ-150C classic anesthesia machine using 4% isoflurane in 1.5 L min^{-1} of O_2 for 4 min prior to surgery. Once anesthetized, rats were prepped by first applying eye ointment to prevent drying, following which an approximately 1×1 in region of the scalp

was shaved. Marcaine (0.25%) was injected subcutaneously to the scalp at the incision site to provide local anesthesia (Table S3). Cefazolin (25 mg kg^{-1}) was injected subcutaneously in the mid-back to prevent infection (Table S3). Toenails were trimmed to prevent the animal from removing sutures.

Surgical procedures closely followed established protocols.[9,46,48] The animal was secured in a Stoelting stereotaxic device under a heating pad, and sedation was maintained using isoflurane (1.75–2.75%) and monitored using a Kent Scientific PhysioSuite vitals monitor. The scalp was cleaned with alternating swabs of chlorohexidine (2%) and isopropanol (70%). A 1-in midline incision was made to the scalp. Eye retractors were inserted to maintain access to the skull. Periosteum was scrubbed away using sterile Q-tips, and the skull was dehydrated using hydrogen peroxide. Instances of persistent bleeding of the periosteum were managed using an electrocautery pen. The stereotaxic device was used to navigate caudal from the Bregma (2 mm for males and 1.5 mm for females) and lateral from the midline on both sides (2 mm); as females were 25–30% smaller, the caudal distance was reduced to ensure implantation into the sensorimotor cortex. A dental drill with a 1.5 mm bit was used for the craniotomy, and the dura was reflected using a 45°-angle pick. An ethylene oxide-sterilized probe was implanted manually into the sensorimotor cortex using fine forceps. Kwik-Cast, a silicone elastomer, was applied over the implant to prevent the brain from drying. Each animal received duplicate probe conditions, either uncoated or PCPC-coated, to ensure that diffusion of coating components would not confound the results of uncoated implants (n = 6–7 animals per coating condition with a minimum of three males and three females per condition). The level of bleeding during drilling, dura reflection, and implantation was noted, and implant sites with excessive bleeding were removed from the study. Vetbond tissue adhesive was spread on the skull to allow adhesion of dental cement. Probes were secured to the skull using dental cement, and the incision was closed using an average of eight stitches with 5–0 prolene Ethicon sutures (8890H).

Immediately after surgery, lidocaine cream and triple antibiotic ointment were applied around the incision site for pain and infection management, respectively. Warm saline (5 mL) and buprenorphine (0.05 mg kg^{-1}) were administered subcutaneously for dehydration and pain management, respectively. Postoperative care and monitoring were provided for 1 week following surgery. Subcutaneous buprenorphine (0.05 mg kg^{-1}) was administered every 4–6 h during the first 12 h postsurgery, with a reduced frequency of every 8–12 h during the following 72 h postsurgery or as needed. Triple antibiotic ointment and lidocaine cream were also applied at each time of injection.

2.11. Tissue Processing.

At the predetermined endpoint of 2 weeks postimplantation, animals were anesthetized with 4% isoflurane in 1.5 L min^{-1} of O_2 for 5 min in the preparation for perfusions. Following which, ketamine (160 mg kg^{-1}) and xylazine (20 mg kg^{-1}) were administered via intraperitoneal injection. Briefly, animals were perfused with warm 1× PBS (700–800 mL) at a rate of 6 mL min^{-1} until the liver was perfused followed by 325 mL of 30% sucrose in 1× PBS for cryopreservation. The brain was carefully removed from the skull and immediately frozen into optimal cutting temperature compound on dry ice for a minimum

of 1 h before being stored at −80 °C for downstream sectioning. The brain was equilibrated using a −20 °C freezer for a minimum of 12 h prior to cryosectioning. Tissue was sectioned using a Leica CM1520 Cryostat at −20 °C. Sequential axial sections were cut 20 μm thick onto unifrost microscope slides through the depth of the probe. Slides were stored at −80 °C until staining.

2.12. Immunohistochemistry.

Samples were thawed for approximately 1 h prior to staining. Brain slices that were approximately 500, 700, 900, 1000, and 1200 μm deep were stained to provide a representative tissue response for the entire mid-section of the probe. Sections were fixed using 4% (v/v) paraformaldehyde (PFA) for 15 min and then washed three times using PBS. Blocking buffer containing 4% (v/v) goat serum and 0.3% (v/v) Triton-X 100 in PBS was applied to sections for 1 h at RT. Sections were then incubated with primary antibody in blocking buffer (Table S5) for 18 h at 4 °C in a humidity chamber to label the cluster of differentiation 68 (CD68) for activated microglia and macrophages, glial fibrillary acidic protein (GFAP) for the astrocytic glial scar, neuronal nuclei (NeuN), and myelin basic protein (MBP). Sections were washed with 1× PBS containing Triton-X 100 (0.1% v/v) six times. Sections were then incubated in blocking buffer containing secondary antibody (Table S6) for 2 h at RT protected from light in a humidity chamber. Sections were incubated in DAPI (1:1000) in PBS containing 0.1% (v/v) Triton-X 100 for 10 min protected from light at RT. Sections were then washed five additional times with PBS containing 0.1% (v/v) Triton-X 100 and three additional times with PBS (1 mL), 5 min per wash. To reduce tissue autofluorescence, brains were treated with copper sulfate buffer (0.5 mM Cu_2SO_4 and 50 mM $NH_4CH_3CO_2$ in deionized water) for 10 min protected from light at RT and then rinsed three times with deionized water. Slides were mounted using Prolong Diamond Anti-Fade mounting medium and covered with a cover glass. Slides were batched stained, grouping animals from the same surgery days that had uncoated and PCPC-coated implants to ensure that all groups were treated the same.

2.13. Confocal Microscopy Imaging of Brain Sections.

An Olympus IX-81 Confocal Microscope and Metamorph Premier 7.7.3.0 imaging software were used to image brain sections. Sections from animals with uncoated probes and animals with PCPC-coated probes were imaged in the same sitting using the same settings (Table S7) to ensure that differences in fluorescence intensity were actually due to a difference in the physiological response. For analysis, images with the implant site centered in the field of view were taken at 4× to ensure a 1-mm radius for analysis around the implant site. The representative images were taken at 10× to better visualize the region around the implant site. Images were taken for the right and left hemispheres of each brain at the depths listed in the Immunohistochemistry section. The researchers imaging the brains were blinded to the treatment group.

2.14. Quantitative Tissue Analysis.

To assess the ability of the PCPC coating to reduce CD68 and MBP levels, normalized fluorescence intensity (± standard error of the mean) was plotted as a function of distance from the implant for each marker. This was achieved using a custom MATLAB code

produced in-house by the Capadona Lab[49] in which implant sites were outlined using the MBP channels. The MATLAB code then assessed the MFI in binned regions extending 5 μm radially from the hole boundary. The code then normalized the MFI for each bin to the MFI for 500–600 μm from the hole boundary as this was deemed healthy tissue. A minimum of four slice depths between 500 and 1200 μm deep were assessed for each brain, resulting in a minimum of 24 implant cross sections analyzed per condition. The researchers outlining the holes were blinded to the treatment group.

2.15. Statistical Analysis.

All data were analyzed in Minitab 19. Data were first assessed for normality using the Ryan–Joiner Test and equal variances when applicable. For profilometry, data were represented as a mean ± standard error of the mean. A two-sample t test was used to assess differences between coated probes and coated wafers. Nanoindentation data were represented as mean ± standard error of the mean. Due to unequal variances, data were compared using Mood's Median Test. For contact angle measurements, data points are represented as mean ± standard error of the mean. Differences at each time point were assessed using a two-sample t test. Wafer fluorescence intensity and total soluble curcumin were represented as mean ± standard error of the mean at each time point.

For immunohistochemical analyses, data taken from each implant side (left and right) and all implant depths (500–600, 600–800, 800–1000, 1000–1200, and 1200–1400 μm) were considered to be technical replicates and were averaged for each animal. Normalized MFI data were fit to a General Linear Model to assess the effect of coating and potential interaction effects of the coating and the confounding variable animal sex. Significance for each coefficient in the model was established at p 0.05. For each treatment (coating condition) or blocked factor (animal sex), there is a term for each factor level: (1) coating – no coating and PCPC coating and (2) sex – female and male. The effect of the PCPC coating (*) and animal sex ⊕ on fluorescence intensity as well as the interaction effect between coating condition and sex ⊕ was assessed with significance established at $p < 0.05$. Data were assessed for normality using the Ryan–Joiner test and equal variances then analysis of variance was also run with post hoc Dunnett's test. Animal designated "ML" was removed from the curcumin group for CD68 and MBP due to staining issues resulting in a high background signal. Detailed statistical data are reported in the Supporting Information.

3. RESULTS AND DISCUSSION

To our knowledge, this is the first study to both synthesize poly(curcumin-PEG$_{1000}$ carbamate) (PCPC) via step-growth polymerization (Figure 1A) and implant nonfunctional probes coated with a curcumin polymer. Before implanting the PCPC-coated nonfunctional probes, the following coating aspects were assessed: (1) morphology and uniformity, (2) mechanical properties, (3) water absorption and swelling, and (4) degradation, dissolution, and antioxidant activity.

3.1. PCPC Synthesis and Characterization.

PCPC was synthesized by step growth polymerization of curcumin and PEG with TDI. Conversion to polymer was evident from the appearance of resonances in the aromatic region 6.75–7.75 ppm in the ^{1}H NMR spectra of the resulting sticky gum-like product (Figure 1B, maroon trace). The weight-average molecular weight was found to be M_w ~ 11 kg/mol ($Đ$ = 1.985) by GPC relative to polystyrene standards (Figure 1C, red). DSC was performed in order to determine the glass transition temperature of the material, which yielded a value of T_g ~ 15 °C (Figure 1D). This thermal transition is far below physiological temperature (37 °C), supporting the notion that the material will exhibit soft, rubbery characteristics when implanted, which is also in good agreement with the nanoindentation data below (Figure 3B).

3.2. PCPC Uniformly Coats Probes.

Electrodes were dip coated with this batch of PCPC polymer. To ensure that PCPC coatings were consistent between batches, nonfunctional probes from each coating batch were imaged using scanning electron and confocal microscopy prior to implantation (Figure 2). Uncoated probes did not fluoresce (Figure 2A, middle) while PCPC-coated probes exhibited fluorescent signals over the entire surface of the probe due to curcumin's native fluorescence, aside from a region of the tab held by the forceps during dip coating (Figure 2B, middle). Accordingly, quantitative analysis demonstrated that 93 ± 5.3% of the probe surface was covered by the PCPC coating. In the probe mplantation model, the top millimeter of the tab remained above the skull and did not interface with brain tissue. SEM showed no change in probe morphology with the PCPC coating (Figure 2B, right) as well as no discernable changes in probe thickness due to the PCPC coating (Figure S2). Quantification of PCPC probe coating thickness using profilometry showed that these coatings were approximately 300 nm thick, increasing probe thickness by approximately 4% (Figure S3).

3.3. PCPC Coating Reduces Hardness of Silicon Wafer.

To minimize tissue damage following implantation, it is important to the minimize mechanical mismatch between the probe interface and the brain, which has an average modulus on the order of 1–2 kPa.[50] In the current study, nanoindentation was used to assess the reduced modulus and hardness of Si wafers and Si wafers with a 1.5 μm-thick PCPC coating (Figure 3A,B). The reduced modulus considers both the elastic deformation of the specimen and the indentation tip and, in this case, is similar to the modulus of the PCPC coating itself due to its significant deformation. The median reduced modulus of the Si wafer (187 GPa with IQR = 28.2 GPa) is approximately 33-fold higher than that of PCPC-coated Si wafer (5.69 GPa with IQR 1.24 GPa) (χ^2 [1] = 6.00, p = 0.014; Figure 3C). Similarly, the median hardness of Si wafer (12.9 GPa with IQR = 0.525 GPa) is approximately 82-fold higher than that of PCPC-coated Si wafer (0.157 GPa with IQR = 0.0394 GPa) (χ [1] = 6.00, p = 0.014; Figure 3D). It is evident that the coating dramatically reduces the mechanical mismatch of the probe. While the coating offers some mechanical benefit, additional improvements are necessary to completely mitigate damage from mechanical mismatch.

3.4. PCPC Coating Absorbs Water with Negligible Swelling.

To assess the hydrophobicity of the PCPC coating, the static water contact angle was measured on both Si and PCPC-coated Si wafers. PCPC appeared to be more hydrophobic than Si, but the contact angle reduced dramatically within 30 s of dropping water on PCPC-coated wafers, with PCPC eventually absorbing water into the coating. From a time course of static water contact angle measurements (Figure 4A,B), droplets on both Si wafer and PCPC-coated Si wafer exhibited spreading over time with a reduction of the mean PCPC contact angle from $96.70 \pm 6.72°$ to $73.06 \pm 3.89°$ after the first 30 s (Figure 4C). After 3 min, the water droplet became irregularly shaped as the polymer absorbed more water, and the contact angle could not be measured. After 2 min, there was no significant difference between the PCPC-coated and uncoated Si wafer measurements (Figure 4C), and the entire water droplet was completely absorbed by the PCPC coating after 15 min.

Based on the absorption of water, there were concerns that the coating would swell significantly, which could increase tissue damage. Thus, successive confocal images were taken of PCPC-coated probes until the absorption equilibrium was reached in $1\times$ PBS (15 min). No major changes in the probe thickness were observed; however, a slight increase in the fluorescence signal of the background was observed, suggesting elution of unreacted curcumin/metabolites (Figure 4D). SEM images were also taken of the PCPC-coated probe before and after a 1-week incubation in deionized water at 37 °C to examine changes in the coating thickness for extended duration at physiological temperature. The surface coating was indistinguishable from the probe surface itself before and after incubation in water, supporting submicron thickness and minimal swelling (Figure 4E), which may be due to intermolecular hydrogen bonding as seen by Dai et al. and Zhang et al.[51,52] This suggests that there is no risk of damaging tissue through increases in the probe thickness. Microscopy also showed no damage to the probe through the dip coating and incubation processes (Figure 4D,E). Future work should assess the effect of PCPC and future coatings on electrode integrity and electrode impedance, as described by Krebs et al.[53]

3.5. PCPC Coating Remains Intact while Releasing PCPC Degradation Products.

To characterize the rate at which PCPC degraded and curcumin or its metabolites were dissolved in solution, PCPC-coated wafers were incubated in $1\times$ PBS at 37 °C for up to 8 weeks and changes in fluorescence of the PBS supernatant as well as the fluorescence signal on the coated wafer were quantified. Despite some delamination of coating from the Si substrate, the PCPC coating remained intact following the 8-week incubation (Figure 5A). Examining a 0.25 mm^2 area of the coating, the sample fields of view show a reduction in MFI over time that stabilized after 1 week. The visible presence of coating and stability of fluorescence signal at 8 weeks suggests that the coating degrades over the scale of months or longer, which may be necessary for treatment and mitigation of chronic probe-induced tissue damage (Figure 5A,B).

To confirm whether the polymerization of curcumin was deemed critical for its stabilization and long-term delivery, a mixture of PEG 10 K and curcumin monomer with the same estimated mole ratio as in PCPC were coated onto probes and wafers. The fluorescence signal of the PEG/curcumin mixture had a dramatically lower intensity than the PCPC

coating. Furthermore, the curcumin was released within an hour of incubation (Figure S4), suggesting that curcumin non-covalently mixed with PEG would not provide sustained curcumin delivery and long-term antioxidant activity.

Despite visualizing an intact coating by photography (Figure 5A), fluorescence voids were visible in the coating after 1 week in PBS (Figure 5B). Microscopic crystallites were observed on the surface of the PCPC coating after 2- and 8-week incubations via SEM (Figure S5). Since curcumin is the source of the fluorescence of PCPC, the images suggest that curcumin monomer, metabolites, or small polymer fragments rich in curcumin have phase separated after aqueous incubation. This hypothesis is further supported by the presence of fluorescent crystals in the PBS supernatant (Figure 5C). These supernatant concentrations were quantified, and after 1 week, approximately 300 nmol of curcumin, metabolites, and/or PCPC oligomer were dissolved in PBS from one coated wafer, leveling off at approximately 1600 nmol at 8 weeks (Figure 5D). Due to the microscale size of intracortical probes for rats, wafers were used to estimate the amount of curcumin, curcumin metabolites, and PCPC oligomers released over time. By dissolving the coating off of the probe and measuring the fluorescence (Figure S6), 240 ± 30 nmol of curcumin were in PCPC on each probe. Based on this, it was estimated that approximately 0.63 nmol of curcumin and curcumin degradation products would release from the probe to local tissue.

Through hydrolytic degradation followed by decarboxylation, we expect that cleavage of the urethane linkages will result in the release of curcumin, as well as the known auto-oxidation byproducts of curcumin.[54–56] In addition, byproducts include PEG and the diaminotoluene derived from the TDI linker unit. At the same time, it has been shown that the curcumin within intact (not degraded) repeating units can still exert antioxidant activity,[57] such that degradation is not a strict prerequisite for activity of the coated films.

We next aimed to confirm that PCPC exhibited antioxidant activities, as studies have shown that curcumin's beneficial effects are due, at least in part, to its antioxidant activity.[26–30] Somparn et al. showed that curcumin metabolites, particularly tetrahydrocurcumin and hexahydrocurcumin, exhibit equal, if not more robust antioxidant activity compared to curcumin itself.[58,59] To confirm PCPC antioxidant activity, its ability to quench radicals was assessed using the free radical compound DPPH. After shaking PCPC in DPPH for 30 min, PCPC quenched the free radical, causing the DPPH solution to lose its purple hue (Figure 5E,F). It is hypothesized that curcumin may mediate oxidative stress via H atom donation from the a carbon or the para hydroxyl.[26,27] Curcumin monomer in pH 7.4 PBS is likely in the enol form,[27] suggesting radical chain-breaking via phenol hydrogen atom donation. As the polymer also appears to exhibit antioxidant activity and the polymerized form does not have phenolic hydrogen atoms to donate, it is likely that there is also chain-breaking via the a hydrogen atom.

3.6. PCPC Demonstrates Similar Biocompatibility to Silicon Nonfunctional Probes.

After in vitro material assessment confirmed a uniform PCPC coating, reduced mechanical mismatch of the probe, and intact coating after 8 weeks, nonfunctional PCPC-coated probes were incubated for up to 1 week within an agarose hydrogel to confirm the coating remained on the probe after mechanical perturbation. Though fluorescence signal intensity was

reduced after incubation in agarose, the coating did not delaminate from the probe during withdrawal from the agarose hydrogel at any time point studied, suggesting some coating stability with probe insertion and removal (Figure S7). This supports that the nanothin coating might be resistant to delamination upon implantation and subsequent micromotion within the brain.

A pilot study was conducted where uncoated and PCPC-coated non-functional probes were implanted into the rat sensorimotor cortex for 2 weeks. Inflammation, glial scarring, neuron loss, and MBP levels were assessed as a function of distance from the implant site using immunohistochemistry. The MFI of binned regions were normalized to the MFI of a 100-μm binned distance of healthy tissue. For all markers assessed at any distance from the implant site, there was no significant difference between the uncoated and PCPC-coated probe groups (Figure 6), indicating no significant change in neuroinflammation, glial scarring, neuron viability, and myelin loss. There was also no significant difference in the implant hole area in response to the coating (Figure S8), further suggesting biocompatibility similar to the silicon probe and lack of toxicity of the newly developed PCPC coating.

While results show similar biocompatibility of the silicon probe and the PCPC-coated probe, suggesting that the coating does not possess additional toxicity, the PCPC coating did not result in statistically significant improvements in the tissue responses as hypothesized (Figure 6). An insignificant trend in myelin basic protein was observed where there was a reduction in MBP staining with the PCPC coating. A study by Gonsalvez et al. suggests that myelin damage increases MBP's antigenicity, resulting in a higher MBP signal by immunostaining,[60] so we expected to see increased MBP in animals with uncoated probes compared to PCPC-coated. We also examined the effect of sex on the response to the PCPC coating; preliminary results show that PCPC may contribute to preservation of myelin in males (Figure S9). While this data is inconclusive due to low statistical power, differences in staining proximal to the implant support future study of sex differences in probe implantation and in response to related therapeutics.

We had hypothesized that the curcumin would reduce neuroinflammation, thereby reducing scarring and neurodegeneration. As this coating did not demonstrate toxicity but also did not demonstrate significant improvement in tissue preservation, the lack of changes observed in tissue responses suggests that there was insufficient curcumin, curcumin lacking bioactivity, or toxic byproducts, resulting in minimal benefit. Future work may optimize the polymer composition and drug incorporation. Understanding challenges with curcumin bioavailability,[25] perhaps an insufficient amount of curcumin was incorporated into this polymer, resulting in no change in tissue inflammation, scarring, and cell death. Future work may consider using both backbone polymerization of and side-chain functionalization with curcumin; the side-chain linkage may allow for burst release of curcumin during the acute tissue injury window (~2 days), while the backbone may be more resistant to degradation, allowing for coating longevity on probes that would be implanted for years in humans. Different polymer architectures may also be assessed, such as dendrimers, to see if curcumin loading efficiency could be increased.[61] Furthermore, future studies may consider using alternative linkers and copolymers to further improve biocompatibility; for example, a recent study in our lab used a sebacoyl linker in place of toluene diisocyanate.[57]

In addition to the incorporation of curcumin, future studies may also incorporate other small molecule anti-inflammatory agents to better target the macrophage and microglia response; for example, research has shown that Itgam, Cd14, and Irak4 play a major role in the innate immune response to electrode implantation[62] and are potential targets for electrode coatings.

4. CONCLUSIONS

Material characteristics of the PCPC coating were thoroughly studied: (1) probes were coated thinly and uniformly with PCPC, showing consistency between batches with no characteristics that would cause additional tissue damage. (2) The PCPC coating reduced the Si modulus and hardness by approximately two orders of magnitude, reducing mechanical mismatch between the probe and brain tissue. (3) The PCPC coating exhibited water absorption but negligible swelling, suggesting that the coating will not cause additional damage to the brain once hydrated. (4) There were high rates of curcumin/curcumin metabolite dissolution during the first 2 weeks following submersion, estimated to elute in amounts that are anti-inflammatory and neuroprotective. The PCPC coating also lasts a minimum of 8 weeks, suggesting antioxidant activity on the time scale of months at the implant site.

To our knowledge, this study was the first to implant nonfunctional intracortical probes coated with a poly(procurcumin). While our results did not show statistically significant differences in histological markers, our findings suggest that the PCPC coating has similar biocompatibility to the control probes. Having a thin, uniform PCPC coating that exhibited minimal swelling likely contributed to the coating's biocompatibility. Finally, electrode mechanical properties should be considered further; the combination of the PCPC coating with in situ softening materials[63,64] may offer promise for minimizing inflammation, scarring, and neuron loss in response to intracortical microelectrode interfaces.

Supplementary Material

Refer to Web version on PubMed Central for supplementary material.

ABBREVIATIONS

BSA	bovine serum albumin
CHCl₃	chloroform
DMSO	dimethyl sulfoxide
FoV	field of view
FITC	fluorescein isothiocyanate
MFI	mean fluorescence intensity
MBP	myelin basic protein
PBS	phosphate buffered saline
PCPC	poly(curcumin-PEG$_{1000}$ carbamate)
PVAc	poly(vinyl acetate)
RT	room temperature
SEM	scanning electron microscopy
Si	silicon

REFERENCES

(1). Fernández E; Greger B; House PA; Aranda I; Botella C; Albisua J; Soto-Sánchez C; Alfaro A; Normann RA Acute Human Brain Responses to Intracortical Microelectrode Arrays: Challenges and Future Prospects. Front. Neuroeng 2014, 7, 24. [PubMed: 25100989]

(2). Jorfi M; Skousen JL; Weder C; Capadona JR Progress Towards Biocompatible Intracortical Microelectrodes for Neural Interfacing Applications. J. Neural Eng 2015, 12, No. 011001.

(3). Hermann JK; Capadona JR Understanding the Role of Innate Immunity in the Response to Intracortical Microelectrodes. Crit. Rev. Biomed. Eng 2018, 46, 341–367. [PubMed: 30806249]

(4). Campbell A; Wu C Chronically Implanted Intracranial Electrodes: Tissue Reaction and Electrical Changes. Micromachines 2018, 9, 430. [PubMed: 30424363]

(5). Biran R; Martin DC; Tresco PA The Brain Tissue Response to Implanted Silicon Microelectrode Arrays Is Increased When the Device Is Tethered to the Skull. J. Biomed. Mater. Res., Part A 2007, 82A, 169–178.

(6). Polikov VS; Tresco PA; Reichert WM Response of Brain Tissue to Chronically Implanted Neural Electrodes. J. Neurosci. Methods 2005, 148, 1–18. [PubMed: 16198003]

(7). Potter-Baker KA; Ravikumar M; Burke AA; Meador WD; Householder KT; Buck AC; Sunil S; Stewart WG; Anna JP; Tomaszewski WH; Capadona JR A Comparison of Neuroinflammation to Implanted Microelectrodes in Rat and Mouse Models. Biomaterials 2014, 35, 5637–5646. [PubMed: 24755527]

(8). Biran R; Martin DC; Tresco PA Neuronal Cell Loss Accompanies the Brain Tissue Response to Chronically Implanted Silicon Microelectrode Arrays. Exp. Neurol 2005, 195, 115–126. [PubMed: 16045910]

(9). Ereifej ES; Rial GM; Hermann JK; Smith CS; Meade SM; Rayyan JM; Chen K; Feng H; Capadona JR Implantation of Neural Probes in the Brain Elicits Oxidative Stress. Front. Bioeng. Biotechnol 2018, 6, 9. [PubMed: 29487848]

(10). Turner JN; Shain W; Szarowski DH; Andersen M; Martins S; Isaacson M; Craighead H Cerebral Astrocyte Response to Micromachined Silicon Implants. Exp. Neurol 1999, 156, 33–49. [PubMed: 10192775]

(11). Thelin J; Jörntell H; Psouni E; Garwicz M; Schouenborg J; Danielsen N; Linsmeier CE Implant Size and Fixation Mode Strongly Influence Tissue Reactions in the CNS. PLoS One 2011, 6, No. e16267.

(12). Kozai TDY; Jaquins-Gerstl AS; Vazquez AL; Michael AC; Cui XT Brain Tissue Responses to Neural Implants Impact Signal Sensitivity and Intervention Strategies. ACS Chem. Neurosci 2015, 6, 48–67. [PubMed: 25546652]

(13). Potter KA; Buck AC; Self WK; Capadona JR Stab Injury and Device Implantation within the Brain Results in Inversely Multiphasic Neuroinflammatory and Neurodegenerative Responses. J. Neural Eng 2012, 9, No. 046020.

(14). McConnell GC; Rees HD; Levey AI; Gutekunst C-A; Gross RE; Bellamkonda RV Implanted Neural Electrodes Cause Chronic, Local Inflammation That Is Correlated with Local Neurodegeneration. J. Neural Eng 2009, 6, No. 056003.

(15). Bedell HW; Capadona JR Anti-Inflammatory Approaches to Mitigate the Neuroinflammatory Response to Brain-Dwelling Intracortical Microelectrodes. J. Immunol. Sci 2018, 2, 15–21. [PubMed: 30854523]

(16). Spataro L; Dilgen J; Retterer S; Spence AJ; Isaacson M; Turner JN; Shain W Dexamethasone Treatment Reduces Astroglia Responses to Inserted Neuroprosthetic Devices in Rat Neocortex. Exp. Neurol 2005, 194, 289–300. [PubMed: 16022859]

(17). Rennaker RL; Miller J; Tang H; Wilson DA Minocycline Increases Quality and Longevity of Chronic Neural Recordings. J. Neural Eng 2007, 4, L1–L5. [PubMed: 17409469]

(18). Potter KA; Buck AC; Self WK; Callanan ME; Sunil S; Capadona JR The Effect of Resveratrol on Neurodegeneration and Blood Brain Barrier Stability Surrounding Intracortical Microelectrodes. Biomaterials 2013, 34, 7001–7015. [PubMed: 23791503]

(19). Potter-Baker KA; Stewart WG; Tomaszewski WH; Wong CT; Meador WD; Ziats NP; Capadona JR Implications of Chronic Daily Anti-Oxidant Administration on the Inflammatory Response to Intracortical Microelectrodes. J. Neural Eng 2015, 12, No. 046002.

(20). Potter-Baker KA; Nguyen JK; Kovach KM; Gitomer MM; Srail TW; Stewart WG; Skousen JL; Capadona JR Development of Superoxide Dismutase Mimetic Surfaces to Reduce Accumulation of Reactive Oxygen Species for Neural Interfacing Applications. J. Mater. Chem. B 2014, 2, 2248–2258. [PubMed: 25132966]

(21). Zhong Y; Bellamkonda RV Dexamethasone Coated Neural Probes Elicit Attenuated Inflammatory Response and Neuronal Loss Compared to Uncoated Neural Probes. Brain Res 2007, 1148, 15–27. [PubMed: 17376408]

(22). Gutowski SM; Shoemaker JT; Templeman KL; Wei Y; Latour RA; Bellamkonda RV; LaPlaca MC; García AJ Protease-Degradable PEG-Maleimide Coating with on-Demand Release of IL-1Ra to Improve Tissue Response to Neural Electrodes. Biomaterials 2015, 44, 55–70. [PubMed: 25617126]

(23). Haley RM; Zuckerman ST; Dakhlallah H; Capadona JR; von Recum HA; Ereifej ES Resveratrol Delivery from Implanted Cyclodextrin Polymers Provides Sustained Antioxidant Effect on Implanted Neural Probes. Int. J. Mol. Sci 2020, 21, 3579. [PubMed: 32438593]

(24). Hewlings SJ; Kalman DS Curcumin: A Review of Its' Effects on Human Health. Foods 2017, 6, 92. [PubMed: 29065496]

(25). Anand P; Kunnumakkara AB; Newman RA; Aggarwal BB Bioavailability of Curcumin: Problems and Promises. Mol. Pharmaceutics 2007, 4, 807–818.

(26). Jovanovic SV; Steenken S; Boone CW; Simic MG H-Atom Transfer Is A Preferred Antioxidant Mechanism of Curcumin. J. Am. Chem. Soc 1999, 121, 9677–9681.

(27). Barclay LRC; Vinqvist MR; Mukai K; Goto H; Hashimoto Y; Tokunaga A; Uno H On the Antioxidant Mechanism of Curcumin: Classical Methods Are Needed To Determine Antioxidant Mechanism and Activity. Org. Lett 2000, 2, 2841–2843. [PubMed: 10964379]

(28). Mythri RB; Jagatha B; Pradhan N; Andersen J; Bharath MMS Mitochondrial Complex I Inhibition in Parkinson's Disease: How Can Curcumin Protect Mitochondria? Antioxid. Redox Signaling 2007, 9, 399–408.

(29). Caillaud M; Chantemargue B; Richard L; Vignaud L; Favreau F; Faye P-A; Vignoles P; Sturtz F; Trouillas P; Vallat J-M; Desmoulière A; Billet F Local Low Dose Curcumin Treatment Improves Functional Recovery and Remyelination in a Rat Model of Sciatic Nerve Crush through Inhibition of Oxidative Stress. Neuropharmacology 2018, 139, 98–116. [PubMed: 30018000]

(30). Gokce EC; Kahveci R; Gokce A; Sargon MF; Kisa U; Aksoy N; Cemil B; Erdogan B Curcumin Attenuates Inflammation, Oxidative Stress, and Ultrastructural Damage Induced by Spinal Cord Ischemia–Reperfusion Injury in Rats. J. Stroke Cerebrovasc. Dis 2016, 25, 1196–1207. [PubMed: 26935117]

(31). Porro C; Cianciulli A; Trotta T; Lofrumento DD; Panaro MA Curcumin Regulates Anti-Inflammatory Responses by JAK/STAT/SOCS Signaling Pathway in BV-2 Microglial Cells. Biology 2019, 8, 51. [PubMed: 31252572]

(32). Jin C; Lee J; Park C; Choi YH; Kim G Curcumin Attenuates the Release of Pro-Inflammatory Cytokines in Lipopolysaccharide-Stimulated BV2 Microglia. Acta Pharmacol. Sin 2007, 28, 1645–1651. [PubMed: 17883952]

(33). Lee HS; Jung KK; Cho JY; Rhee MH; Hong S; Kwon M; Kim SH; Kang SY Neuroprotective Effect of Curcumin Is Mainly Mediated by Blockade of Microglial Cell Activation. Pharmazie 2007, 62, 937–942. [PubMed: 18214347]

(34). Yu Y; Shen Q; Lai Y; Park SY; Ou X; Lin D; Jin M; Zhang W Anti-Inflammatory Effects of Curcumin in Microglial Cells. Front. Pharmacol 2018, 9, 386. [PubMed: 29731715]

(35). Kim HY; Park EJ; Joe E-H; Jou I Curcumin Suppresses Janus Kinase-STAT Inflammatory Signaling through Activation of Src Homology 2 Domain-Containing Tyrosine Phosphatase 2 in Brain Microglia. J. Immunol 2003, 171, 6072–6079. [PubMed: 14634121]

(36). Potter KA; Jorfi M; Householder KT; Foster EJ; Weder C; Capadona JR Curcumin-Releasing Mechanically Adaptive Intracortical Implants Improve the Proximal Neuronal Density and Blood-Brain Barrier Stability. Acta Biomater. 2014, 10, 2209–2222. [PubMed: 24468582]

(37). Nguyen JK Investigation of Material and Therapeutic Strategies to Reduce the Inflammatory Response to Intracortical Implants; Case Western Reserve University, 2015. https://etd.ohiolink.edu/pg_10?0::NO:10:P10_ACCESSION_NUM:case1431086131 (accessed August 29, 2020).

(38). Requejo-Aguilar R; Alastrue-Agudo A; Cases-Villar M; Lopez-Mocholi E; England R; Vicent MJ; Moreno-Manzano V Combined Polymer-Curcumin Conjugate and Ependymal Progenitor/Stem Cell Treatment Enhances Spinal Cord Injury Functional Recovery. Biomaterials 2017, 113, 18–30. [PubMed: 27810639]

(39). Matsumi N; Nakamura N; Aoi K Novel Bio-Based Polyesters Derived from Curcumin as an Inherent Natural Diol Monomer. Polym. J 2008, 40, 400–401.

(40). Tang H; Murphy CJ; Zhang B; Shen Y; Van Kirk EA; Murdoch WJ; Radosz M Curcumin Polymers as Anticancer Conjugates. Biomaterials 2010, 31, 7139–7149. [PubMed: 20591475]

(41). Shpaisman N; Sheihet L; Bushman J; Winters J; Kohn J One-Step Synthesis of Biodegradable Curcumin-Derived Hydrogels as Potential Soft Tissue Fillers after Breast Cancer Surgery. Biomacromolecules 2012, 13, 2279–2286. [PubMed: 22703560]

(42). Ghosh AK; Brindisi M Organic Carbamates in Drug Design and Medicinal Chemistry. J. Med. Chem 2015, 58, 2895–2940. [PubMed: 25565044]

(43). Luo J; Borgens R; Shi R Polyethylene Glycol Immediately Repairs Neuronal Membranes and Inhibits Free Radical Production after Acute Spinal Cord Injury. J. Neurochem 2002, 83, 471–480. [PubMed: 12423257]

(44). Xie F; Zhang T; Bryant P; Kurusingal V; Colwell JM; Laycock B Degradation and Stabilization of Polyurethane Elastomers. Prog. Polym. Sci 2019, 90, 211–268.

(45). Ziemba AM Characterization of Intracortical Microelectrode Coatings to Mitigate Scarring and Neurodegeneration in Vivo; Ph.D.; Rensselaer Polytechnic Institute: United States -- New York, 2020. https://search.proquest.com/docview/2438962113/abstract/B112080A015F48EAPQ/1 (accessed September 29, 2020).

(46). Ereifej ES; Smith CS; Meade SM; Chen K; Feng H; Capadona JR The Neuroinflammatory Response to Nanopatterning Parallel Grooves into the Surface Structure of Intracortical Microelectrodes. Adv. Funct. Mater 2018, 28, No. 1704420.

(47). McCutcheon JE; Marinelli M Age Matters. Eur. J. Neurosci 2009, 29, 997–1014. [PubMed: 19291226]

(48). Mahajan S; Hermann JK; Bedell HW; Sharkins JA; Chen L; Chen K; Meade SM; Smith CS; Rayyan J; Feng H; Kim Y; Schiefer MA; Taylor DM; Capadona JR; Ereifej ES Toward Standardization of Electrophysiology and Computational Tissue Strain in Rodent Intracortical Microelectrode Models. Front. Bioeng. Biotechnol 2020, 8, 416. [PubMed: 32457888]

(49). Goss-Varley M; Dona KR; McMahon JA; Shoffstall AJ; Ereifej ES; Lindner SC; Capadona JR Microelectrode Implantation in Motor Cortex Causes Fine Motor Deficit: Implications on Potential Considerations to Brain Computer Interfacing and Human Augmentation. Sci. Rep 2017, 7, 15254. [PubMed: 29127346]

(50). Budday S; Nay R; de Rooij R; Steinmann P; Wyrobek T; Ovaert TC; Kuhl E Mechanical Properties of Gray and White Matter Brain Tissue by Indentation. J. Mech. Behav. Biomed. Mater 2015, 46, 318–330. [PubMed: 25819199]

(51). Zhang Q; Wang X; Cong Y; Kang Y; Wu Z; Li L Conjugated Polymer-Functionalized Stretchable Supramolecular Hydrogels to Monitor and Control Cellular Behavior. ACS Appl. Mater. Interfaces 2022, 14, 12674–12683. [PubMed: 35235302]

(52). Dai X; Zhang Y; Gao L; Bai T; Wang W; Cui Y; Liu W A Mechanically Strong, Highly Stable, Thermoplastic, and Self-Healable Supramolecular Polymer Hydrogel. Adv. Mater 2015, 27, 3566–3571. [PubMed: 25946310]

(53). Krebs OK; Mittal G; Ramani S; Zhang J; Shoffstall AJ; Cogan SF; Pancrazio JJ; Capadona JR Tools for Surface Treatment of Silicon Planar Intracortical Microelectrodes. J. Visualized Exp 2022, 184.

(54). Griesser M; Pistis V; Suzuki T; Tejera N; Pratt DA; Schneider C Autoxidative and Cyclooxygenase-2 Catalyzed Transformation of the Dietary Chemopreventive Agent Curcumin. J. Biol. Chem 2011, 286, 1114–1124. [PubMed: 21071447]

(55). Gordon ON; Schneider C Vanillin and Ferulic Acid Are Not the Major Degradation Products of Curcumin. Trends Mol. Med 2012, 18, 361–363. [PubMed: 22652257]

(56). Gordon ON; Luis PB; Sintim HO; Schneider C Unraveling Curcumin Degradation: Autoxidation Proceeds through Spiroepoxide and Vinylether Intermediates En Route to the Main Bicyclopentadione. J. Biol. Chem 2015, 290, 4817–4828. [PubMed: 25564617]

(57). Chen R; Funnell JL; Quinones GB; Bentley M; Capadona JR; Gilbert RJ; Palermo EF Poly(pro-Curcumin) Materials Exhibit Dual Release Rates and Prolonged Antioxidant Activity as Thin Films and Self-Assembled Particles. Biomacromolecules 2023, 24, 294–307. [PubMed: 36512693]

(58). Somparn P; Phisalaphong C; Nakornchai S; Unchern S; Morales NP Comparative Antioxidant Activities of Curcumin and Its Demethoxy and Hydrogenated Derivatives. Biol. Pharm. Bull 2007, 30, 74–78. [PubMed: 17202663]

(59). Shen L; Ji H-F The Pharmacology of Curcumin: Is It the Degradation Products? Trends Mol. Med 2012, 18, 138–144. [PubMed: 22386732]

(60). Gonsalvez DG; Yoo S; Fletcher JL; Wood RJ; Craig GA; Murray SS; Xiao J Imaging and Quantification of Myelin Integrity After Injury With Spectral Confocal Reflectance Microscopy. Front. Mol. Neurosci 2019, 12, 275. [PubMed: 31803018]

(61). Liechty WB; Kryscio DR; Slaughter BV; Peppas NA Polymers for Drug Delivery Systems. Annu. Rev. Chem. Biomol. Eng 2010, 1, 149–173. [PubMed: 22432577]

(62). Bedell HW; Schaub NJ; Capadona JR; Ereifej ES Differential Expression of Genes Involved in the Acute Innate Immune Response to Intracortical Microelectrodes. Acta Biomater. 2020, 102, 205–219. [PubMed: 31733330]

(63). Capadona JR; Shanmuganathan K; Tyler DJ; Rowan SJ; Weder C Stimuli-Responsive Polymer Nanocomposites Inspired by the Sea Cucumber Dermis. Science 2008, 319, 1370–1374. [PubMed: 18323449]

(64). Jorfi M; Roberts MN; Foster EJ; Weder C Physiologically Responsive, Mechanically Adaptive Bio-Nanocomposites for Biomedical Applications. ACS Appl. Mater. Interfaces 2013, 5, 1517–1526. [PubMed: 23379302]
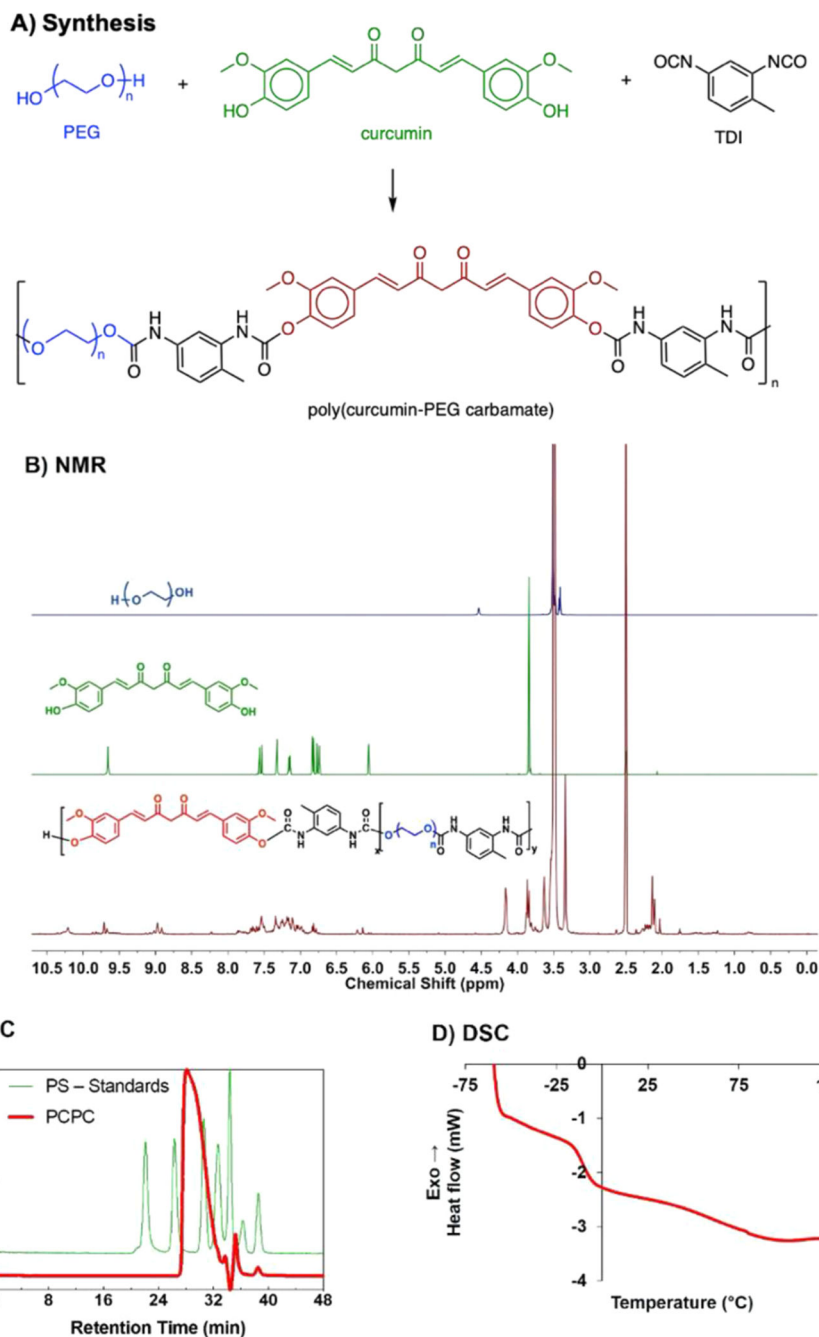
Figure 1.
Curcumin was successfully polymerized to synthesize poly(curcumin-PEG$_{1000}$ carbamate). (A) Reaction scheme of PCPC synthesis via step-growth polymerization. (B) ^{1}H NMR of PEG$_{1000}$ (top), curcumin (middle), and PCPC (bottom) in DMSO-d$_6$. (C) Gel permeation chromatography of PCPC (red) in THF. PCPC molecular weight was then determined using monodisperse polystyrene standards (green). (D) Representative PCPC sample DSC curve.
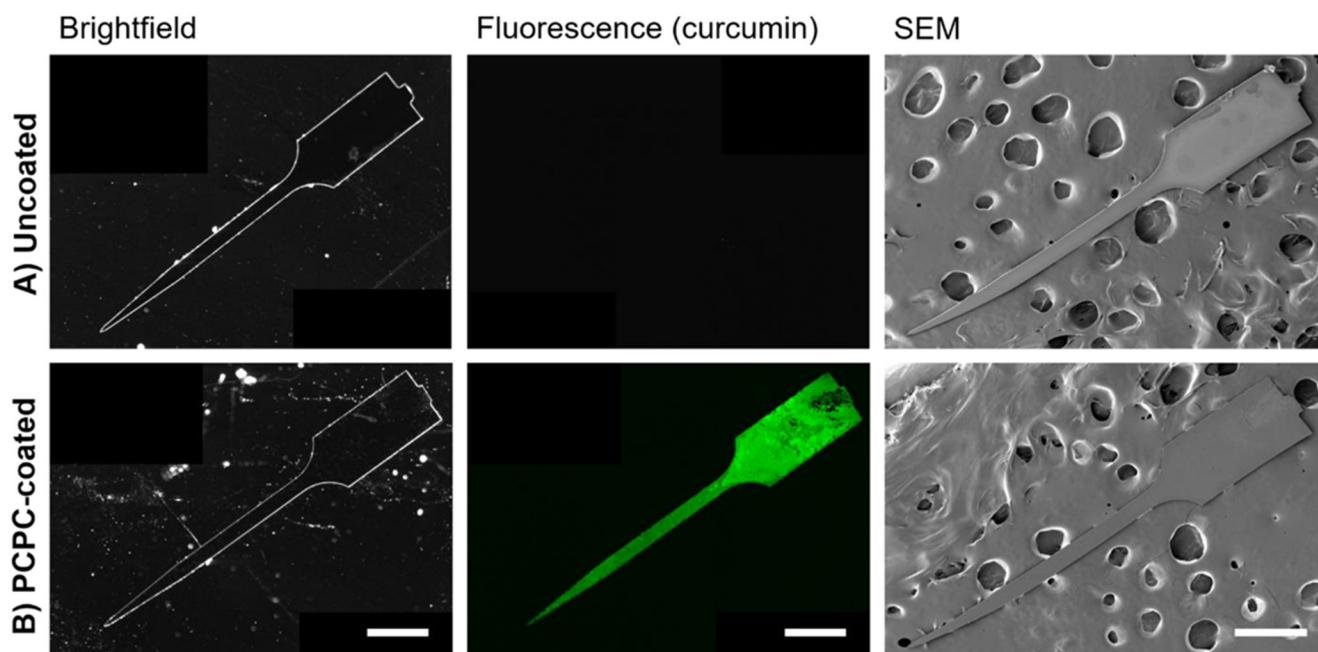
Figure 2.
Microscopy of probe demonstrates uniform PCPC coating. Fluorescence microscopy of the native curcumin signal and scanning electron microscopy show that the morphologies of (A) uncoated and (B) PCPC-coated probes are similar ($n = 6$ probes with 1–2 probes from each batch assessed prior to implantation for quality control; all scale bars = 500 μm).
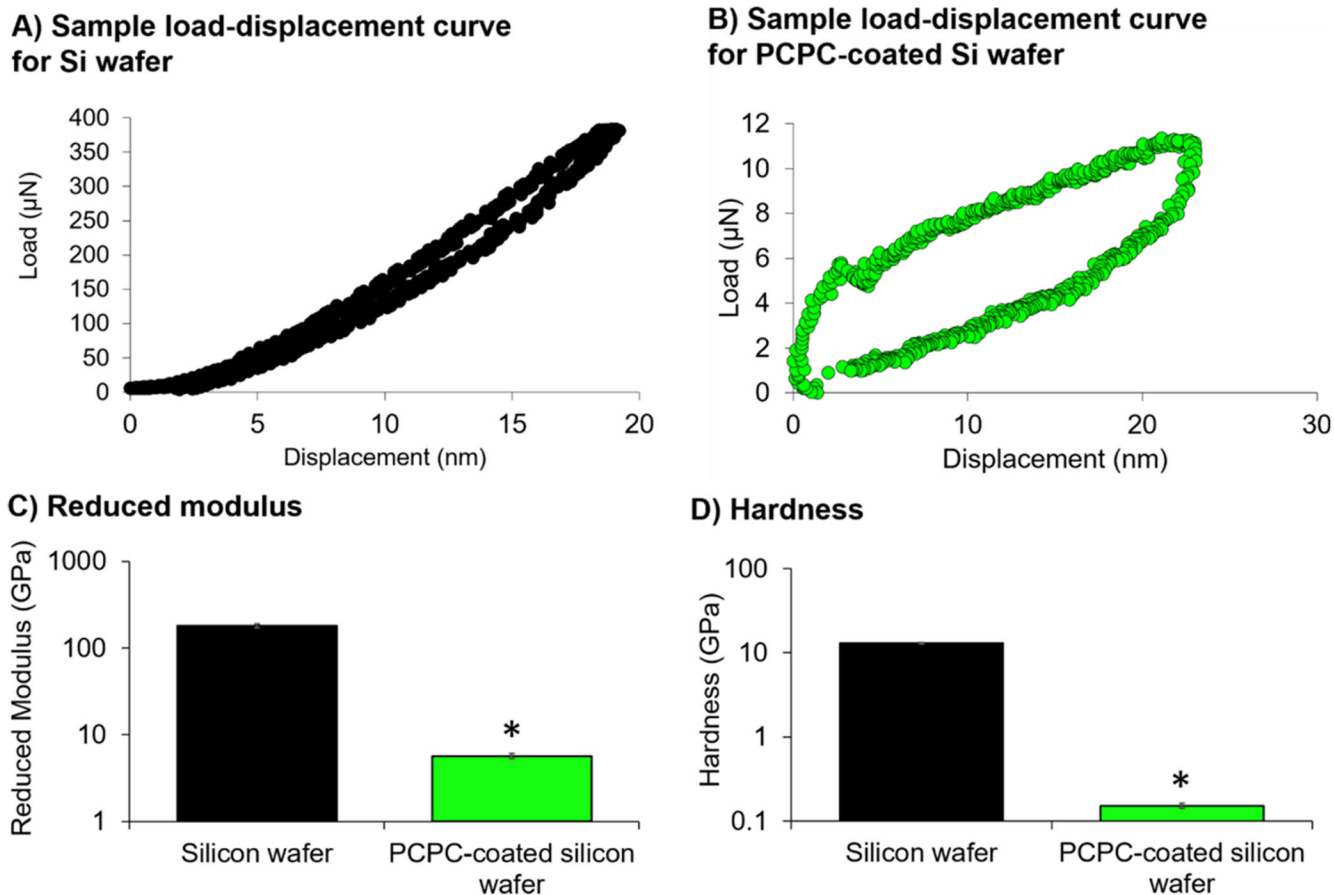
Figure 3.
PCPC-coatings have significantly lower reduced modulus and hardness than silicon wafers. Sample load–displacement curve for (A) Si wafer and (B) PCPC-coated Si wafer. (C) Reduced modulus and (D) hardness summary plots are represented as mean ± standard error of the mean ($n = 3$ separate wafers with a minimum of 11 technical replicate measurements taken per sample). Statistical differences between PCPC-coated Si and uncoated Si wafers were assessed using a Mood's Median test (*$p < 0.05$).
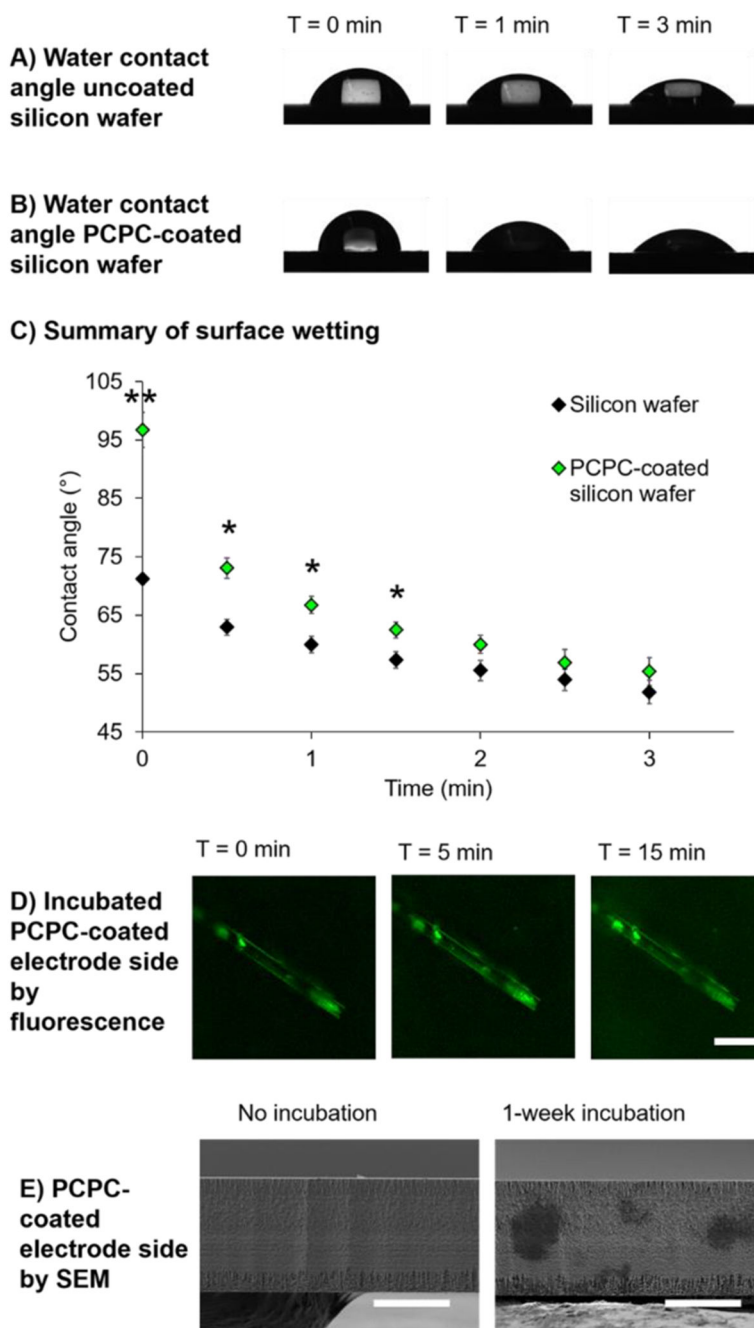
Figure 4.

PCPC-coated wafer quickly absorbs water with minimal swelling after water absorption equilibrium has been reached. Sample images of 3 μL static water contact angle measurements for (A) uncoated and (B) PCPC-coated Si wafer from 0 to 3 min following placement of water droplets. (C) Summary graph showing mean ± standard error of the mean of water contact angle at each time point (n = 3–5 PCPC-coated wafers per time point). Two-sample t tests were conducted at each time point to assess the difference in contact angle between uncoated and PCPC-coated Si wafers (*p 0.001, $p < 0.05$). (D)

Sample fluorescence images of the PCPC-coated probe at $T = 0$, 5, and 15 min post-diH$_2$O incubation (scale bar = 50 μm). (E) Sample SEM images of the 15 μm thick probe side to show the thickness of coating on the top surface without and with a 1-week incubation in diH$_2$O at 37 °C (scale bars = 10 μm).
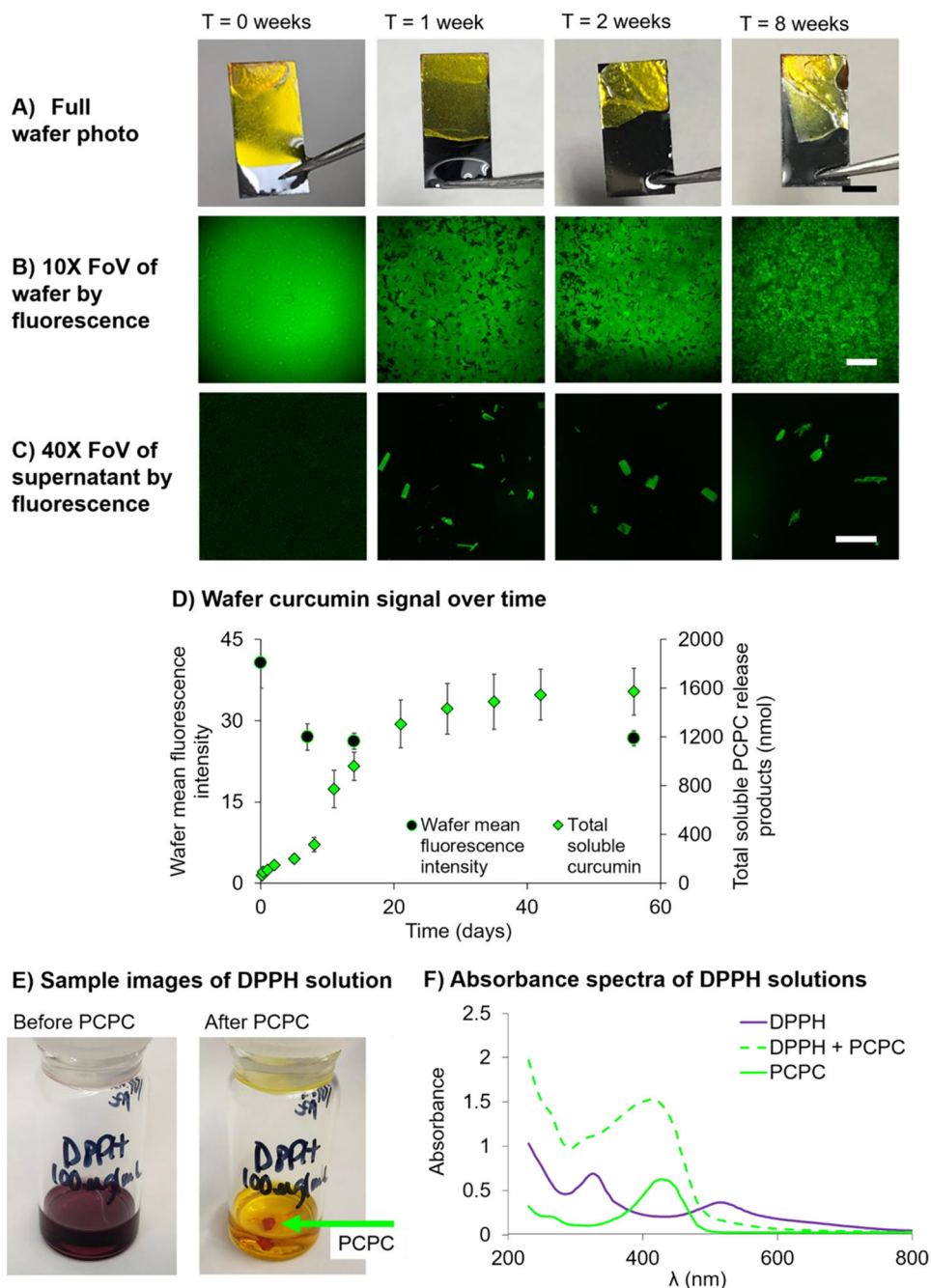
Figure 5.
Degradation/dissolution of PCPC occurs during the first 2 weeks and continues at a slow rate up to 8 weeks. (A) Sample images of entire PCPC-coated wafers at 0, 1, 2, and 8 weeks post-PBS incubation (scale bar = 5 mm). (B) Sample 10× FoV of PCPC-coated wafers at 0, 1, 2, and 8 weeks post-PBS incubation (scale bar = 150 μm). (C) Sample 40× FoV of the wafer-incubated PBS supernatants at 0, 1, 2, and 8 weeks post-PBS incubation (scale bar = 50 μm). (D) Summary plot displays changes in the fluorescence signal over time for PCPC release products dissolved in the PBS supernatant in nmol (green diamonds) and wafer

PCPC coating as MFI (black circles). Data are represented as mean ± standard error of the mean (*n* = measurements from three PCPC-coated wafers or supernatants per time point). (E) Sample images of DPPH solution (100 μg/mL in 100% ethanol) and DPPH solution 30 min post-PCPC incubation exhibiting PCPC antioxidant activity. (F) Absorbance spectrum of DPPH, DPPH + PCPC, and PCPC solutions.
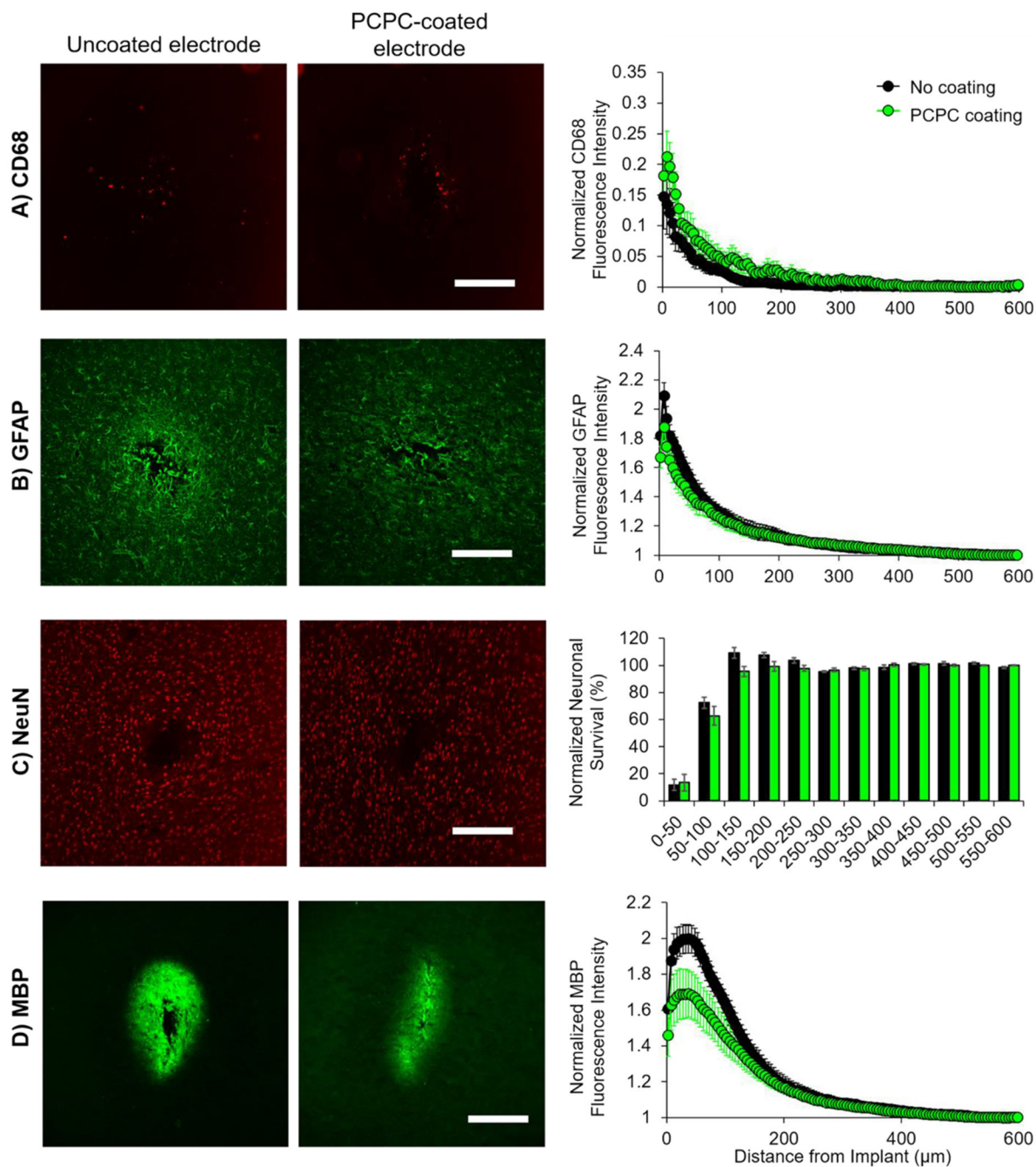
Figure 6.
PCPC coating demonstrates similar biocompatibility to nonfunctional silicon implants. (A) Presence of activated microglia and macrophages was assessed through staining against CD68, (B) astrocytic scarring levels were assessed through staining against GFAP, (C) neuron loss was assessed through staining neuronal nuclei using NeuN, and (D) myelin damage was assessed through staining against MBP. Sample confocal micrographs of brain tissue that had either uncoated probes (left) or PCPC-coated probes (right) in female rats. Sample images were taken at 10× magnification with the same settings (scale bars =

200 μm). For A, B, and D, summary plots display the normalized fluorescence intensity (normalized to 500–600 μm binned radius from hole) as a function of the distance from the implant hole. For C, the summary plot displays the normalized neuronal survival (normalized to 500–600 μm binned radius from hole) as a function of the distance from the implant hole. For all, data are represented as mean ± standard error of the mean. Statistical significance between uncoated (black) and PCPC-coated (green) probe groups was assessed using a General Linear Model ($n = 3$ female no coating, 3 female PCPC coating, 3 male no coating, 3 male PCPC coating).